On the computations of interatomic Coulombic decay widths with R-matrix method

Nicolas Sisourat, Selma Engin, Jimena D. Gorfinkiel, Sévan Kazandjian, Přemysl Kolorenč, and Tsveta Miteva

Citation: The Journal of Chemical Physics **146**, 244109 (2017); doi: 10.1063/1.4989538
View online: http://dx.doi.org/10.1063/1.4989538
View Table of Contents: http://aip.scitation.org/toc/jcp/146/24
Published by the American Institute of Physics

On the computations of interatomic Coulombic decay widths with R-matrix method

Nicolas Sisourat,[1,a)] Selma Engin,[1] Jimena D. Gorfinkiel,[2] Sévan Kazandjian,[1] Přemysl Kolorenč,[3] and Tsveta Miteva[1]

[1]*Sorbonne Universités, UPMC Univ Paris 06, CNRS, Laboratoire de Chimie Physique Matière et Rayonnement, F-75005 Paris, France*

[2]*School of Physical Sciences, The Open University, Walton Hall, Milton Keynes MK7 6AA, United Kingdom*

[3]*Charles University, Faculty of Mathematics and Physics, Institute of Theoretical Physics, V Holešovičkách 2, 180 00 Prague, Czech Republic*

(Received 5 May 2017; accepted 9 June 2017; published online 27 June 2017)

Interatomic Coulombic Decay (ICD) is a general mechanism in which an excited atom can transfer its excess energy to a neighbor which is thus ionized. ICD belongs to the family of Feshbach resonance processes, and, as such, states undergoing ICD are characterized by their energy width. In this work, we investigate the computations of ICD widths using the R-matrix method as implemented in the UKRmol package. Helium dimer is used here as a benchmark system. The results are compared with those obtained with the well established Fano-Algebraic Diagrammatic Construction method. It is shown that the R-matrix method in its present implementation provides accurate total and partial widths if the kinetic energy of the ICD electron is lower than 10 eV. Advantages and limitations of the R-matrix method on the computations of ICD widths are discussed. *Published by AIP Publishing.* [http://dx.doi.org/10.1063/1.4989538]

I. INTRODUCTION

Interatomic (Intermolecular) Coulombic Decay (ICD) is an efficient non-radiative electronic relaxation mechanism for excited atoms and molecules embedded in a chemical environment.[1–3] By means of ICD, the excited system transfers its excess energy to a neighboring atom or molecule which is thus ionized. ICD has been investigated theoretically and experimentally in rare-gas clusters, hydrogen-bonded systems, and liquid phase (see Refs. 4–6 for recent reviews).

Depending on the system, ICD takes place on the femtosecond to picosecond time scales and it is generally the dominant decay pathway unless local Auger decay is operative. While this general characteristic of ICD is well established,[7] computing accurately the lifetime of the excited species, or turning from time to energy domain, the energy width of the corresponding state, remains challenging. Several methods have been implemented to compute *ab initio* ICD widths of ionized and/or excited atoms and molecules in small clusters. Semi-quantitative estimates at the lowest order of perturbation theory can be obtained using the Wigner-Weisskopf method.[8] More accurate approaches currently used can be classified into two groups. The first one relies on the Fano-Feshbach description of a resonant state as a "discrete state in a continuum,"[9,10] encompassing, namely, Fano-CI (Configuration Interaction)[11] and Fano-ADC (Algebraic Diagrammatic Construction)[12–14] methods. The second group comprises techniques combining Complex Absorbing Potential (CAP) and tools from excited-state quantum-chemistry, such as CI,[15] ADC,[16] or coupled cluster method.[17] Besides these *ab initio* methods, it should be mentioned that analytical formulas for ICD widths, which are valid when the atoms and molecules are sufficiently far apart, have been derived.[18,19]

In many systems, several ICD channels are open leading to different final states. In order to have a complete description of ICD processes, the partial widths (corresponding to different channels) are needed. A common feature of all the aforementioned methods is the use of square-integrable (L^2) basis sets. The lack of true continuum wave functions, however, hinders proper characterization of the decay channels, as they are only defined asymptotically with respect to the outgoing electron. Approximate schemes have been developed to compute partial widths using the Fano-Feshbach approaches, while methods relying on the CAP provide only total ICD widths. Accurate computations of partial widths are therefore needed to test the approximate schemes of the former methods.

R-matrix methods[20–22] correspond to another class of theoretical approaches to compute resonance energy widths. These methods have been successfully employed for studying resonances in electron-atom and electron-molecule collisions. Furthermore, in contrast to the Fano-Feshbach and CAP approaches, the different decay channels are well defined in R-matrix methods. The latter are therefore better suited for the computations of partial widths.

In this work, we use the R-matrix method as implemented in the UKRmol package[23] to compute the total and partial ICD widths in helium dimer. ICD in helium dimer has been theoretically and experimentally investigated.[24–29] In helium dimer, ICD is triggered by simultaneous ionization and excitation of one helium atom within the dimer. The excited ion transfers its excess energy to the other helium atom which is ionized. In this study, we focus on ICD after ionization and excitation

a)Nicolas.Sisourat@upmc.fr

into the $2p$ orbitals of He^+,

$$\begin{aligned} He - He + h\nu &\rightarrow He^+(2p) - He + e_{ph} \\ &\rightarrow He^+(1s) + He^+(1s) + e_{ICD} + e_{ph}, \end{aligned}$$

where e_{ph} and e_{ICD} are the so-called photoelectron and ICD electron, respectively.

The computational costs of the R-matrix method increase substantially with the number of channels and the energy of the ICD electron. It should be noted that in the case of helium dimer, there are only two channels for each resonance, corresponding to singlet and triplet $He^+(1s) + He^+(1s)$ final states. Furthermore, the ICD electron has kinetic energy below 20 eV. Helium dimer is therefore a good candidate system for applying the R-matrix method.

The outline of the article is the following: in Sec. II, we briefly describe the R-matrix method employed to compute the total and partial ICD widths and we provide the computational details. In Sec. III, the total and partial ICD widths computed with the R-matrix method are compared to the data obtained with the Fano-ADC approach. The article ends with the conclusions of this work. Atomic units are used throughout the article, unless stated otherwise.

II. METHODS AND COMPUTATIONAL DETAILS

Since R-matrix methods have been recently reviewed in Ref. 21 and details of the UKRmol package are reported in Ref. 23, here we only summarize the method and the implementation used in this work.

In the R-matrix method, the configuration space is partitioned into an inner and an outer region separated by a sphere of radius a centered at the center of mass of the system. The inner region contains the multielectron description of the so-called (N-electron) target states and of a free scattered electron. Thus all $N + 1$ electrons are considered explicitly in this region. In the outer region, only the single scattered electron is treated, and the interaction of this particle with the target is described in terms of a multipole expansion. The R-matrix links the two regions. In the case of ICD, the target states included in the calculations are the *final states* of the ICD process. In helium dimer, they correspond to singlet and triplet $He^+(1s) + He^+(1s)$ states. The scattered particle considered in the outer region is the ICD electron.

The first step of the calculations is to obtain the eigenvalues and eigenvectors of $(H - L)$, where H is the electronic Hamiltonian and L is the Bloch operator.[22,30] For a system having $N + 1$ electrons, the eigenfunctions are written as

$$\begin{aligned} \Psi_k(\mathbf{x_1}, \mathbf{x_2}, \ldots, \mathbf{x_{N+1}}) = A \sum_{ij} \alpha_{ijk} \phi_i(\mathbf{x_1}, \mathbf{x_2}, \ldots, \mathbf{x_N}) u_{ij}(\mathbf{x_{N+1}}) \\ + \sum_i \beta_{ik} \chi_i(\mathbf{x_1}, \mathbf{x_2}, \ldots, \mathbf{x_{N+1}}), \end{aligned} \quad (1)$$

where the operator A ensures that the wave functions are antisymmetric with respect to interchange of two electrons, $\phi_i(\mathbf{x_1}, \mathbf{x_2}, \ldots, \mathbf{x_N})$ are the target states, u_{ij} are the continuum-like orbitals which describe the scattered electron within the inner region, and χ_i are the so-called L^2 configurations. The latter configurations account for the correlation between the N target electrons and the scattering one. These configurations are crucial for the description of Feshbach resonances. The spatial and spin coordinates of electron i are denoted as $\mathbf{x_i}$. The coefficients α_{ijk} and β_{ik} and the associated eigenvalues E_k are obtained by diagonalizing $(H - L)$ in the corresponding basis sets.

The energy dependent R-matrix at the boundary a between the inner and outer regions is obtained from these eigenvalues and eigenvectors in the following way:

$$R_{ij}(E, a) = \frac{1}{2a} \sum_k \frac{w_{ik}(a) w_{jk}(a)}{E_k - E}, \quad (2)$$

where E is the energy of the scattered particle and the sum runs over all eigenstates defined in Eq. (1). The boundary amplitudes w_{ik} for channel i are defined by

$$w_{ik}(a) = \sum_j \alpha_{ijk} u_{ij}(a). \quad (3)$$

Note that spin integration has been performed in Eq. (3), and thus the boundary amplitudes depend only on the spatial coordinates of the scattered particle.

The R-matrix is then propagated from distance a to a larger distance from the center of mass of the molecule, where it is matched with asymptotic solutions of known form. From this, the K-matrices which contain all information on the scattering process are obtained.[20,21] The total resonance width may be obtained in several ways.[21] Here we use the program RESON[31] which fits the eigenphase sums $\delta(E)$ with a Breit-Wigner profile. The eigenphase sum is obtained by

$$\delta(E) = \sum_i \arctan(k_i), \quad (4)$$

where k_i are the eigenvalues of the corresponding K-matrix. A Breit-Wigner profile is defined as

$$\delta(E) = \delta_0(E) + \arctan \frac{\Gamma}{2(E_r - E)}, \quad (5)$$

where E_r and Γ are the resonance energy position and width, respectively. The background contribution $\delta_0(E)$ is usually a smooth function of energy. The partial widths are obtained using the program TIMEDEL[32] which uses the S-matrices built from the K-matrices to calculate the time-delay matrix.[33]

In the case of ICD, the target states correspond to the ICD final states, while the decaying states are described by the L^2 configurations. The CI expansions used to describe the target states as well as the L^2 configurations included in the calculations are detailed hereafter.

The configurations included in the description of the target states and in the scattering calculations are denoted relative to a reference electronic configuration which is here the Hartree-Fock determinant for neutral He_2: $|\Phi_0\rangle = |\sigma_g \bar{\sigma}_g \sigma_u \bar{\sigma}_u|$. In the following, we compare the results of two different schemes:

- In the first scheme, the target states are obtained by diagonalizing the Hamiltonian matrix constructed in the basis of all spin-adapted 2 hole (2h) configurations (e.g., $c_{\sigma_g} c_{\bar{\sigma}_g} |\Phi_0\rangle$, where c_i denotes the annihilation operator). Similarly, the L^2 configurations comprise all possible spin-adapted 2 hole–1 particle (2h1p) configurations (where 1p is the virtual orbital occupied by the excited electron). Such a level of description is equivalent to the ADC scheme used in the Fano-ADC calculations.[26]

- In the second scheme, higher-order configurations are employed: spin-adapted 2h and 3h1p configurations are used to describe the target states, whereas the scattering states are described with 2h1p and 3h2p configurations. With this scheme we investigate the convergence of the ICD widths with respect to the CI expansions.

We used Restricted Hartree-Fock (RHF) molecular orbitals for neutral He_2 optimized with the MOLPRO package.[34,35] In order to check the convergence with respect to the Gaussian type orbital basis sets, we performed the calculations with the aug-cc-pv5z and the aug-cc-pv6z basis sets.[36] All virtual orbitals were included in the active space. The same continuum-like orbitals u_{ij} were used in both schemes: 151 continuum-like orbitals centered in between the two helium atoms. The continuum-like orbitals are described as linear combinations of Gaussian functions (11s 10p 10d 8f 6g) and are chosen to be orthogonal to the RHF molecular orbitals. The Gaussian functions were optimized for $a = 6.88$ Å.[37]

For the outer region calculations, the R-matrix is propagated from $a = 6.88$ Å to 42 Å, which is sufficient for obtaining converged K-matrices (i.e., the same results are obtained with propagation to larger distances). The maximum multipole to be retained in the expansion of the long range potential is set to 2. The ukrmol-in-1.0 and ukrmol-out-0.0 release versions of the UKRmol package were used.

III. RESULTS

A. Total ICD widths

There are four states corresponding to $He^+(2p) - He$, denoted $^2\Sigma_g^+$, $^2\Sigma_u^+$, $^2\Pi_g$, and $^2\Pi_u$. As shown below, the widths for each of these states depend strongly on the interatomic distance (R). We first discuss the results for $R = 2$ Å, which is around the equilibrium distance of the ionized-excited helium dimer.[26] Furthermore, we compare the results obtained with the Fano-ADC and the R-matrix (using scheme 1) methods. Effects of higher-order configurations (scheme 2) are discussed in Sec. III C.

The eigenphase sums [Eq. (4)] obtained with the aug-cc-pv5z and aug-cc-pv6z basis sets for Π_g symmetry are shown in Fig. 1. For both basis sets, the eigenphase sums clearly exhibit two Breit-Wigner profiles indicating the presence of resonances. Only one of these resonances corresponds to a state prepared by ionizing and exciting one helium atom within the dimer. The $He^+(2p) - He$ Π_g state as well as the ICD final states are expected to be well described within the two basis sets, and the resonance position should not vary substantially. The resonance located around 7 eV is thus attributed to the $He^+(2p) - He$ Π_g state. The other resonance has an energy width which is too large to correspond to ICD, and, furthermore, its position changes significantly with the basis set. This resonance is related to the scattering of an incoming electron on two singly charged helium ions and is not relevant for the present study.

The eigenphase sums around the relevant resonance are shown in the inset of Fig. 1 for the aug-cc-pv5z basis set. A fit with Eq. (5) for which $\delta_0(E)$ is taken as a linear function of E gives the resonance position at 7.25 eV and an energy width of 8 meV.

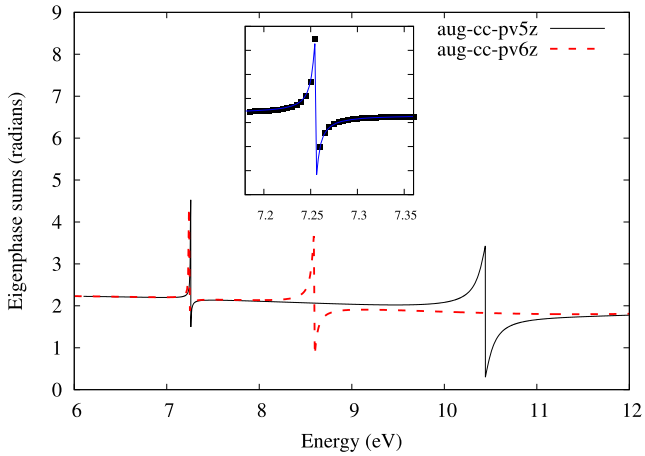

FIG. 1. Eigenphase sums for Π_g symmetry obtained with the aug-cc-pv5z and aug-cc-pv6z basis sets (scheme 1) at $R = 2$ Å. The energy E is given with respect to the energy of the lowest target state. The eigenphase sums exhibit two Breit-Wigner profiles indicating resonances. The resonance located at 7.25 eV corresponds to ICD from the $He^+(2p) - He$ state. The inset shows the eigenphase sums (black square) around the relevant resonance for the aug-cc-pv5z basis set. The full blue line in the inset shows the fit with Eq. (5) for which $\delta_0(E)$ is taken as a linear function of E.

The same procedure is applied to the three other states ($^2\Sigma_g^+$, $^2\Sigma_u^+$, $^2\Pi_u$). The total widths for the two basis sets are summarized and compared to the Fano-ADC calculations (see Ref. 26) in Table I. The comparison shows that the results are converged with respect to the Gaussian basis sets. Furthermore, the results from the Fano-ADC calculations agree with the first scheme used in the R-matrix calculations: the widths from the R-matrix differ by less than 25% compared to the Fano-ADC results. It should be noted that the R-matrix calculations with the first scheme and the Fano-ADC calculations include both only 2h1p configurations for describing the scattering states. This comparison shows that at a similar level of the CI expansion, the Fano-ADC and the R-matrix methods provide comparable total widths.

In order to compare further the Fano-ADC and the R-matrix approaches, we have computed the total ICD widths for several interatomic distances. For the R-matrix calculations, we have used the aug-cc-pv5z basis set. The total ICD widths for all $He^+(2p) - He$ states are shown in Fig. 2. There is a quantitative agreement between the two approaches for interatomic distances below 4 Å, particularly for the Π_g and Π_u states. However, above $R = 4$ Å, the widths calculated using the R-matrix decrease faster compared to the Fano-ADC results.

TABLE I. Total widths (in meV) of $He^+(2p) - He$ states for $R = 2$ Å. Scheme 1 corresponds to 2h and 2h1p configurations for the target states and L^2 configurations, respectively (2h1p configurations are used in the Fano-ADC calculations).

	Γ (meV)			
	$^2\Sigma_g^+$	$^2\Sigma_u^+$	$^2\Pi_g$	$^2\Pi_u$
Fano-ADC[26]	24	16	9	24
Scheme 1 (aug-cc-pv5z)	23	12	8	24
Scheme 1 (aug-cc-pv6z)	25	12	8	23

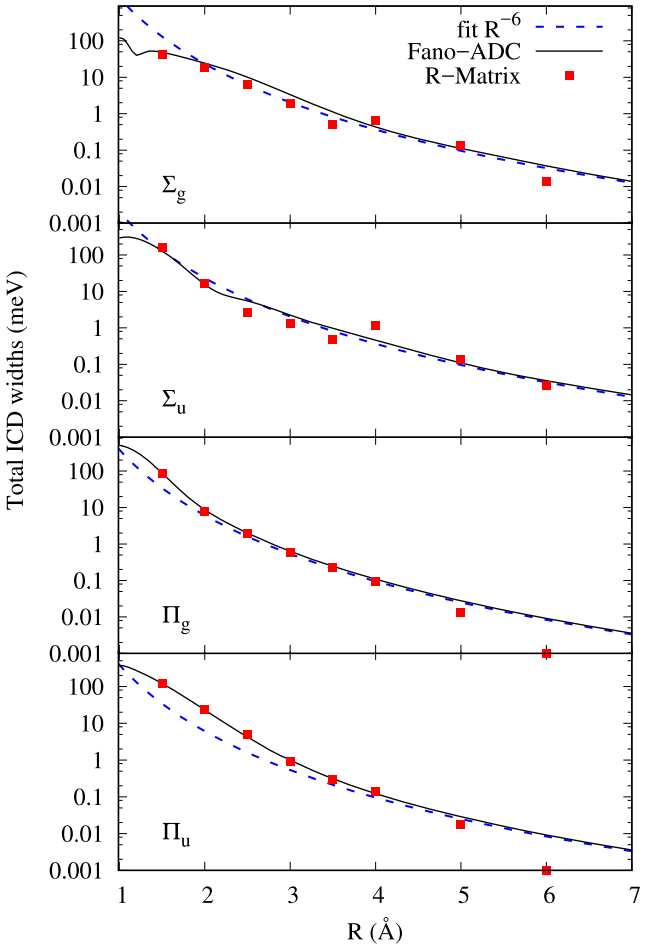

FIG. 2. Total ICD widths (in meV) of $He^+(2p)$ – He states as functions of the interatomic distance. Scheme 1 and the aug-cc-pv5z basis set were used for the R-matrix calculations. Asymptotically, the ICD widths are expected to decrease like $1/R^6$ which is shown by the dashed blue line.

The slightly worse agreement between the two approaches for the Σ states is probably due to the presence of energetically nearly degenerate states of the same symmetry corresponding to the initial excitation into the 2*s* orbital because the mixing between the 2*p*-like and 2*s*-like Σ resonances is not described exactly equivalently in the two methods.

At large interatomic distances, the ICD process can be described as two separate dipole transitions, where the initially excited species relaxes by emitting a *virtual* photon, which is then absorbed by the neighbor and the neighbor is ionized. Within this virtual photon approximation, the ICD widths are expected to decrease like $1/R^6$,[18,19] which is well reproduced only by the Fano-ADC calculations. The failure of the R-matrix method to reproduce the long-range behavior of the decay widths is to be attributed to the insufficient number of continuum-like orbitals included in the inner-region calculations. The kinetic energy of the ICD electron increases at large distances which cannot be described accurately with the present set of continuum-like orbitals. To show this, we have computed the ICD widths with the Fano-ADC method but with the same basis set as in the R-matrix calculations. The results for the Π_u state are compared with those obtained with a much larger Gaussian basis set (see Ref. 26 for details) in Fig. 3. The ICD widths obtained with the two basis sets are nearly equal

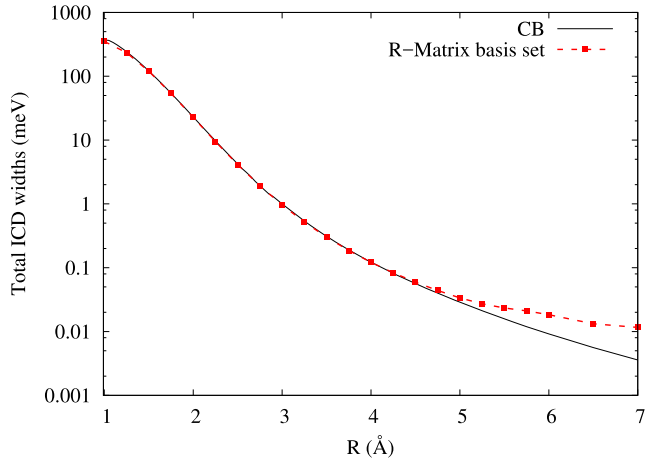

FIG. 3. Total ICD widths (in meV) of $He^+(2p)$ – He Π_u state as functions of the interatomic distance obtained with the Fano-ADC method. Results with the same basis set as in the R-matrix calculations (red dashed line) are compared to that obtained with a converged basis set (CB, black line) at all distances.

below 4 Å and start to differ above this distance. The same trends are observed for the three other states. This comparison allows us to determine an upper limit to the kinetic energy of the ICD electron that can be considered with the UKRmol implementation of the method. The limit is about 10 eV, corresponding to the resonance position relative to the target states at $R = 3.5$ Å.

B. Partial ICD widths

A more thorough comparison between the Fano-ADC and the R-matrix approaches is provided by the partial widths. The branching ratios for the singlet and triplet $He^+(1s)$ + $He^+(1s)$ final states are shown in Table II at $R = 2$ Å. The results confirm that the partial widths obtained with the R-matrix method are converged with respect to the basis set. Furthermore, there is a quantitative agreement with the branching ratios computed using the Fano-ADC method. These results indicate that the approximate scheme used in the Fano-ADC method is reliable at this level of description (see Refs. 12 and 26 for more details on the computations of partial widths with the Fano-ADC method).

We now discuss the singlet/triplet branching ratios in the interatomic distance range for which the R-matrix calculations are valid (R ≤ 3.5 Å). The singlet branching ratios as functions of the interatomic distances are shown in Fig. 4. For the R-matrix calculations, the aug-cc-pv5z basis set was used. For $^2\Sigma_u^+$, $^2\Pi_g$, and $^2\Pi_u$ states, both methods predict similar trends: at short interatomic distances, the singlet final state corresponds to the stronger or even dominant decay channel. It should be mentioned that this is generally the case for Auger

TABLE II. Singlet/Triplet branching ratios of the $He^+(2p)$ – He states at interatomic distance R = 2 Å. The R-matrix ratios are obtained using the program TIMEDEL.[32]

	$^2\Sigma_g^+$	$^2\Sigma_u^+$	$^2\Pi_g$	$^2\Pi_u$
Fano-ADC[26]	0.34/0.66	0.40/0.60	0.33/0.67	0.61/0.39
Scheme 1 (aug-cc-pv5z)	0.38/0.62	0.45/0.55	0.28/0.72	0.58/0.42
Scheme 1 (aug-cc-pv6z)	0.39/0.61	0.47/0.53	0.28/0.72	0.59/0.41

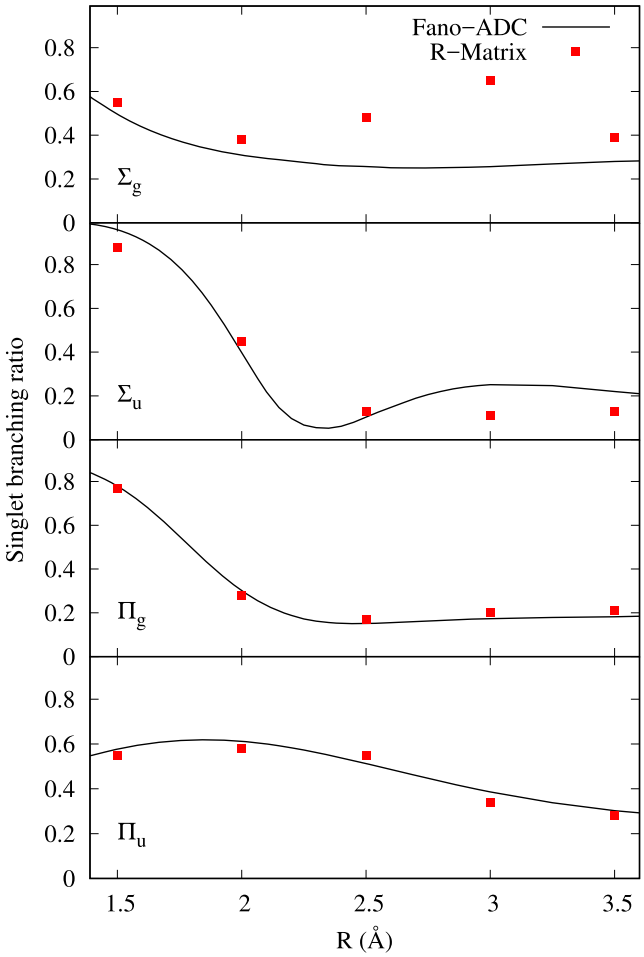

FIG. 4. Singlet branching ratios of the $He^+(2p)$ – He states obtained with the R-matrix (red squares) and the Fano-ADC (black line) approaches. For the R-matrix calculations, scheme 1 and the aug-cc-pv5z basis set were used.

decay in molecules.[38,39] On the contrary, at large interatomic distances, the triplet final state is more populated after ICD than the singlet one, as expected in the virtual photon approximation.[18,19] For the $^2\Sigma_g^+$ state, the R-matrix method predicts an increase in the singlet branching ratio for interatomic distances around 2.5-3 Å, while the branching ratios computed with the Fano-ADC method are nearly constant. There is no obvious explanation for such a disagreement, and no conclusions on whether one or the other method provides more accurate partial decay widths for the $^2\Sigma_g^+$ state can be drawn here.

C. Higher-order configurations

In contrast to the Fano-ADC method, including higher-order configurations is straightforward in R-matrix calculations. However, when these configurations are added to the description of the target and scattering states (scheme 2), the resonance energy position (at all interatomic distances) is shifted by about +2.5 eV compared to that obtained with scheme 1. This blue shift limits the interatomic distance range that can be investigated with the set of continuum-like orbitals employed here. In scheme 2, the ICD electron energy is higher than 10 eV already for distances above 2 Å. Therefore, the total ICD widths and the branching ratios are shown only for the shortest distances in Tables III and IV, respectively.

TABLE III. Total ICD widths (in meV) of the $He^+(2p)$ – He states obtained with the R-matrix method and scheme 2. For comparison, the total ICD widths obtained with scheme 1 are reported in parentheses. For both schemes, the aug-cc-pv5z basis set was used.

	Γ (meV)			
R (Å)	$^2\Sigma_g^+$	$^2\Sigma_u^+$	$^2\Pi_g$	$^2\Pi_u$
1.5	36 (44)	136 (165)	82 (86)	84 (120)
2	17 (23)	28 (12)	5 (8)	18 (24)

TABLE IV. Singlet branching ratios of the $He^+(2p)$ – He states obtained with the R-matrix method and scheme 2. For comparison, the results obtained with scheme 1 are reported in parentheses. For both schemes, the aug-cc-pv5z basis set was used.

R (Å)	$^2\Sigma_g^+$	$^2\Sigma_u^+$	$^2\Pi_g$	$^2\Pi_u$
1.5	0.95 (0.55)	0.65 (0.88)	0.81 (0.77)	0.74 (0.55)
2	0.58 (0.38)	0.14 (0.45)	0.43 (0.28)	0.82 (0.58)

The comparison between scheme 1 and 2 in Table III shows that the computed widths differ significantly when higher-order configurations are included. Except for the $^2\Sigma_u^+$ state at $R = 2$ Å, the widths obtained with scheme 2 are smaller. The effects of higher-order configurations are also seen in the partial ICD widths. As seen in Table IV, while the predicted dominant decay channel is the same for both schemes, the branching ratios differ quantitatively, showing a rather strong effect of the higher-order configurations.

It should be mentioned that the corrections due to these configurations go beyond a simple shift of the resonance energy position. To illustrate this, we artificially applied an energy shift to the resonance position in the Fano-ADC calculations which results in minor changes in total and partial ICD widths: the total ICD widths change by less than 12% and the branching ratio is nearly unaffected for all states.

We recall that in scheme 1, 2h and 2h1p configurations are used in the description of the target and scattering states, respectively. In scheme 2, the target and scattering states are described with 2h-3h1p and 2h1p-3h2p configurations, respectively. It should be mentioned that if 3h1p configurations are used in the description of the target states without adding 3h2p configurations in the scattering states (or vice versa), no Breit-Wigner profiles are seen in the eigenphase sums. This is probably due to a strong unbalanced description of the target and the scattering states, as discussed in Ref. 21.

IV. CONCLUSIONS

In conclusion, we have employed the R-matrix method as implemented in the UKRmol package to compute the total and partial ICD widths of the $He^+(2p)$ – He states. The results were compared to the well-established Fano-ADC approach. Using the same class of configurations, both approaches provide similar widths. However, the R-matrix method allows us to include straightforwardly higher-order configurations. We have demonstrated that the latter have a rather strong effect on both total and partial widths. Finally, we have shown that the R-matrix method in its present implementation is significantly limited concerning the kinetic energy of the ICD electron. In

particular, the continuum-like basis set used in the present work is insufficient if the kinetic energy of the ICD electron exceeds 10 eV. However, a new implementation of the method, the UKRmol+ suite, enables the accurate description of the continuum for significantly higher energies[40] (either by the inclusion of B-splines or the use of quadruple precision in the integral calculation) and should overcome this limitation.

The R-matrix method has some advantages compared to the Fano-ADC approach: first the R-matrix method relies on the use of true continuum states, while the Fano-ADC approach uses L^2 states and must employ Stieltjes imaging procedure to extract continuum quantities. Second, the R-matrix approach provides a rigorous framework to compute the partial widths, while only approximate schemes have been derived for Fano-ADC. Third, as shown in the present study, higher-order configurations can be included while keeping a balanced description between resonance and target states. Finally, the UKRmol package has been used to compute the angular distribution of photoelectrons.[41] The R-matrix method could therefore provide the angular distribution of the ICD electron.

ACKNOWLEDGMENTS

This project has received funding from the Research Executive Agency (REA) under the European Union's Horizon 2020 research and innovation programme Grant agreement No 705515 and from Agence Nationale de la Recherche through the program No. ANR-16-CE29-0016-01. P.K. acknowledges financial support from the Czech Science Foundation (Project GAČR No. 17-10866S).

[1] L. S. Cederbaum, J. Zobeley, and F. Tarantelli, Phys. Rev. Lett. **79**, 4778 (1997).
[2] S. Marburger, O. Kugeler, U. Hergenhahn, and T. Möller, Phys. Rev. Lett. **90**, 203401 (2003).
[3] T. Jahnke, A. Czasch, M. S. Schöffler, S. Schössler, A. Knapp, M. Käsz, J. Titze, C. Wimmer, K. Kreidi, R. E. Grisenti, A. Staudte, O. Jagutzki, U. Hergenhahn, H. Schmidt-Böcking, and R. Dörner, Phys. Rev. Lett. **93**, 163401 (2004).
[4] U. Hergenhahn, J. Electron Spectrosc. Relat. Phenom. **184**, 78 (2011).
[5] U. Hergenhahn, Int. J. Radiat. Biol. **88**, 871 (2012).
[6] T. Jahnke, J. Phys. B: At., Mol. Opt. Phys. **48**, 082001 (2015).
[7] U. Frühling, F. Trinter, F. Karimi, J. B. Williams, and T. Jahnke, J. Electron Spectrosc. Relat. Phenom. **204**, 237 (2015).
[8] R. Santra and L. S. Cederbaum, Phys. Rep. **368**, 1 (2002).
[9] U. Fano, Phys. Rev. **124**, 1866 (1961).
[10] H. Feshbach, Rev. Mod. Phys. **36**, 1076 (1964).
[11] T. Miteva, S. Kazandjian, and N. Sisourat, Chem. Phys. **482**, 208 (2017).
[12] V. Averbukh and L. S. Cederbaum, J. Chem. Phys. **123**, 204107 (2005).
[13] P. Kolorenč and N. Sisourat, J. Chem. Phys. **143**, 224310 (2015).
[14] E. Fasshauer, P. Kolorenč, and M. Pernpointner, J. Chem. Phys. **142**, 144106 (2015).
[15] R. Santra and L. S. Cederbaum, J. Chem. Phys. **115**, 6853 (2001).
[16] N. Vaval and L. S. Cederbaum, J. Chem. Phys. **126**, 164110 (2007).
[17] Y. Sajeev, A. Ghosh, N. Vaval, and S. Pal, Int. Rev. Phys. Chem. **33**, 397 (2014).
[18] V. Averbukh, I. B. Müller, and L. S. Cederbaum, Phys. Rev. Lett. **93**, 263002 (2004).
[19] K. Gokhberg, S. Kopelke, N. V. Kryzhevoi, P. Kolorenč, and L. S. Cederbaum, Phys. Rev. A **81**, 013417 (2010).
[20] P. G. Burke and J. Tennyson, Mol. Phys. **103**, 2537 (2005).
[21] J. Tennyson, Phys. Rep. **491**, 29 (2010).
[22] P. G. Burke, *R-Matrix Theory of Atomic Collisions: Application to Atomic, Molecular and Optical Processes* (Springer, 2011).
[23] J. Carr, P. Galiatsatos, J. Gorfinkiel, A. Harvey, M. Lysaght, D. Madden, Z. Mašin, M. Plummer, J. Tennyson, and H. Varambhia, Eur. Phys. J. D **66**, 58 (2012).
[24] N. Sisourat, N. V. Kryzhevoi, P. Kolorenč, S. Scheit, T. Jahnke, and L. S. Cederbaum, Nat. Phys. **6**, 508 (2010).
[25] N. Sisourat, N. V. Kryzhevoi, P. Kolorenč, S. Scheit, and L. S. Cederbaum, Phys. Rev. A **82**, 053401 (2010).
[26] P. Kolorenč, N. V. Kryzhevoi, N. Sisourat, and L. S. Cederbaum, Phys. Rev. A **82**, 013422 (2010).
[27] T. Havermeier, T. Jahnke, K. Kreidi, R. Wallauer, S. Voss, M. Schöffler, S. Schössler, L. Foucar, N. Neumann, J. Titze, H. Sann, M. Kühnel, J. Voigtsberger, J. H. Morilla, W. Schöllkopf, H. Schmidt-Böcking, R. E. Grisenti, and R. Dörner, Phys. Rev. Lett. **104**, 133401 (2010).
[28] T. Havermeier, K. Kreidi, R. Wallauer, S. Voss, M. Schöffler, S. Schössler, L. Foucar, N. Neumann, J. Titze, H. Sann, M. Kühnel, J. Voigtsberger, N. Sisourat, W. Schöllkopf, H. Schmidt-Böcking, R. E. Grisenti, R. Dörner, and T. Jahnke, Phys. Rev. A **82**, 063405 (2010).
[29] F. Trinter, J. B. Williams, M. Weller, M. Waitz, M. Pitzer, J. Voigtsberger, C. Schober, G. Kastirke, C. Müller, C. Goihl, P. Burzynski, F. Wiegandt, T. Bauer, R. Wallauer, H. Sann, A. Kalinin, L. Schmidt, M. Schöffler, N. Sisourat, and T. Jahnke, Phys. Rev. Lett. **111**, 093401 (2013).
[30] C. Bloch, Nucl. Phys. **4**, 503 (1957).
[31] J. Tennyson and C. J. Noble, Comput. Phys. Commun. **33**, 421 (1984).
[32] D. T. Stibbe and J. Tennyson, Comput. Phys. Commun. **114**, 236 (1998).
[33] F. T. Smith, Phys. Rev. **118**, 349 (1960).
[34] H.-J. Werner, P. J. Knowles, G. Knizia, F. R. Manby, and M. Schütz, Wiley Interdiscip. Rev.: Comput. Mol. Sci. **2**, 242 (2012).
[35] H.-J. Werner, P. J. Knowles, G. Knizia, F. R. Manby, M. Schütz, P. Celani, W. Györffy, D. Kats, T. Korona, R. Lindh, A. Mitrushenkov, G. Rauhut, K. R. Shamasundar, T. B. Adler, R. D. Amos, A. Bernhardsson, A. Berning, D. L. Cooper, M. J. O. Deegan, A. J. Dobbyn, F. Eckert, E. Goll, C. Hampel, A. Hesselmann, G. Hetzer, T. Hrenar, G. Jansen, C. Köppl, Y. Liu, A. W. Lloyd, R. A. Mata, A. J. May, S. J. McNicholas, W. Meyer, M. E. Mura, A. Nicklass, D. P. O'Neill, P. Palmieri, D. Peng, K. Pflüger, R. Pitzer, M. Reiher, T. Shiozaki, H. Stoll, A. J. Stone, R. Tarroni, T. Thorsteinsson, and M. Wang, MOLPRO, version 2015.1, a package of *ab initio* programs, 2015, see http://www.molpro.net .
[36] D. E. Woon and T. H. Dunning, Jr., J. Chem. Phys. **100**, 2975 (1994).
[37] A. Faure, J. D. Gorfinkiel, L. A. Morgan, and J. Tennyson, Comput. Phys. Commun. **144**, 224 (2002).
[38] H. Ågren, J. Chem. Phys. **75**, 1267 (1981).
[39] F. Tarantelli, A. Sgamellotti, L. S. Cederbaum, and J. Schirmer, J. Chem. Phys. **86**, 2201 (1987).
[40] D. S. Brambila, A. G. Harvey, Z. Mašín, J. D. Gorfinkiel, and O. Smirnova, J. Phys. B: At., Mol. Opt. Phys. **48**, 245101 (2015).
[41] A. G. Harvey, D. S. Brambila, F. Morales, and O. Smirnova, J. Phys. B: At., Mol. Opt. Phys. **47**, 215005 (2014).